Temperature-dependent diffusive to ballistic transport transition in aligned double walled carbon nanotubes in the high frequency regime

George Chimowa, Emmanuel Flahaut, Somnath Bhattacharyya

Temperature-dependent diffusive to ballistic transport transition in aligned double walled carbon nanotubes in the high frequency regime

George Chimowa,[1] Emmanuel Flahaut,[2] and Somnath Bhattacharyya[1,a)]
[1]*Nano-Scale Transport Physics Laboratory, School of Physics, and DST- NRF Centre of Excellence in Strong materials, University of the Witwatersrand, Johannesburg, South Africa*
[2]*Université Paul Sabatier, CNRS, Institut Carnot Cirimat, 118, route de Narbonne, F-31062 Toulouse, Cedex 9, France*

Low-temperature induced diffusive to ballistic transport in aligned double walled carbon nanotubes (DWNT) is reported. This is evidenced by a crossover of the imaginary (reactive) component of the alternating current impedance being greater than the real (resistive) component, which happens in the range of 9 GHz–1.5 GHz at temperatures77 K and 4 K from which we estimate a long lifetime of 17 ps and 106 ps in DWNTs, respectively. By simulating the measured scattering parameters of a few aligned DWNTs over a wide temperature range, we show that this observation is strongly influenced by the electrode–DWNT coupling strength.
[http://dx.doi.org/10.1063/1.4901025]

Electrical transport properties of carbon nanotubes (CNTs) are commonly measured after acid purification, surfactant stabilization, and ultrasonification dispersion prior to the deposition of electrodes. These processes can lead to defects and doping of the outerwall in the CNTs which affects the transport mechanism. This is probably why most catalytically produced and lithographically contacted CNTs have been found to be diffusive at room temperature.[1,2] Coherent transport has been observed in singlewalled (SWNT) and multi-walled nanotubes (MWNT) at cryogenic temperatures with the exception of pristine MWNTs measured using an *in-situ* microscopy technique.[3] Transport in SWNTs that are often aligned on top of insulating substrates is influenced by substrate surface roughness as in some graphene devices.[4] Furthermore, multi-walled nanotubes and SWNT networks may suffer from multiple conduction channels depending on the contacting technique.[5] This may make it difficult to compare with theoretical models that assume simplified, strict one-dimensional (1D) channel assumptions. Unlike SWNTs and MWNTs, double walled carbon nanotubes (DWNTs) have only two walls which offer a platform to study ballistic transport features that have been demonstrated in freely suspended pristine multi-walled nanotubes.[3] Earlier experimental and theoretical works on filled DWNTs have shown that these nanotubes demonstrate unique1D features due to the nearly structurally perfect inner wall that is protected by the outer wall.[6,7] The inner wall thus remains unaffected by the chemical purification processes, and substrate interference effects although the outer wall of DWNTs can be biased in such a manner it behaves as a gate.[8] However, the alignment of the tubes is necessary to observe 1D transport which can be affected by the interaction of tubes in a bundle of CNTs.[5,9–11] In this letter using on-wafer probing on coplanar waveguides (which has now become the standard technique for measuring the scattering (S)-parameters of nano-materials), we show the possibility of 1D ballistic conduction through the alternating current (AC) impedance of a few horizontally aligned DWNTs.

In previous works on high frequency properties of dense DWNTs networks, fabricated by ink-jet printing onto the waveguide, a strong frequency dependence of DWNTs microwave parameters as well as abrupt changes in effective permittivity was observed. This property could be used in gas sensor applications.[9–11] We extended this work by probing few aligned tubes so as to unearth any unique quantum features regarding this strong frequency dependence. The ideal scenario would be to measure a single tube but unfortunately because of the inherent load mismatch a minimum of four parallel DWNTs was used. This improves the output signal by reducing the effective (quantum) resistance from $\sim$13 kΩ to $\sim$3 kΩ for four CNTs in parallel. This configuration is equivalent to a bundle consisting of a few weakly coupled tubes in parallel. While there is still significant mismatch with the waveguide, the signal level is nevertheless improved greatly.[5,10,11]

Ideally ballistic transport is regarded as the motion of charge carriers without any scattering; however, contact resistance always inhibits this. We however have attempted to achieve ballistic transport in two ways: (i) reducing the sample dimensions to the range of the mean free path[12] or (ii) using a time-dependent signal whose frequency is greater than the scattering rate in the material. In this case, the effect of local defect centres to transport can be reduced. The Drude model for frequency (ω) dependent transport expresses the conductivity (σ) made of two parts; the real part and imaginary parts given by $\sigma(\omega) = \frac{ne^2\tau}{m^*}\frac{1}{1+i\omega\tau}$, where τ, m^*,e, and n represent the momentum scattering time, effective electron mass, electronic charge, and the carrier density, respectively.[13] The imaginary part of the conductivity is given by $i\omega\tau$ and it changes sign depending on whether it is capacitive or inductive. We can therefore make use of this fact to determine experimentally whether the transport is the diffusive or ballistic regime if the real and imaginary impedance is known. To complement AC response measurements, two-terminal direct (DC) current-voltage (I-V) measurements

a)Author to whom correspondence should be addressed. Electronic mail: Somnath.Bhattacharyya@wits.ac.za

were performed and fitted with the Landauer-Büttiker theory, which describes the transmission of electrons from the electrode to the CNT as:

$$I(V) = \frac{2e}{h}\int_{-\infty}^{+\infty} \frac{\Gamma^2}{(E-\Delta E)^2+\Gamma^2} \times \left[f_F\left(E - E_F - \frac{eV}{2}\right) - f_F\left(E - E_F + \frac{eV}{2}\right)\right] dE, \quad (1)$$

where ΔE and f_F are the energy difference of the CNT from electrode Fermi energy level (E_F) and the Fermi distribution function, respectively.[14] This analysis is very important to determine the strength of CNT-electrode coupling (Γ) and subsequently the nature of electrical conduction in these devices, namely the crossover of real and imaginary parts of impedance at different temperatures.

DWNTs were synthesized by Catalytic Chemical Vapour Deposition (CCVD) for more details see Ref. 15. Finally, they were dispersed in ($\sim$0.013 mg/cm^3) dichlorobenzene and prepared for high frequency S- parameter measurements by aligning them on 1 mm long coplanar waveguide (CPW) with a 1 μm gap using dielectrophoresis, which is known to favour alignment of metallic CNTs.[16] Kleindek nanomanipulators in the scanning electron microscope (SEM) were used to remove unwanted CNTs and large bundles.[17] Some of actual SEM micrographs of the devices that were used for HF measurement are shown in Fig. 1(a). The CNTs appear as dark sheds on the waveguide because of charging effects during imaging since the gap is non-conductive. The transmission electron microscope (TEM) image Fig. 1(b) illustrates the high quality of the unaligned DWNT bundles before transferring them for device fabrication.[17]

S-parameter measurements were done using an Agilent Precision Network Analyser (PNA) E8361C at room and low temperatures under vacuum (10^{-5} millibar) for more details and instrument calibration see references.[17,18] The temperature dependent I-V measurements were done using the Agilent B1500A semiconductor analyser with a 1 pA resolution. Measurement parasitic (i.e., effects due to the substrate) were extracted by using the open-short de-embedding method an industrially accepted technique, see the Eq. (2) below[19]

$$Y_{DUT} = [(Y_{msd} - Y_{open})^{-1} - (Y_{short} - Y_{open})^{-1}]^{-1}, \quad (2)$$

where Y_{msd} is the measured admittance of the CPW plus the aligned CNT, Y_{open} and Y_{short} are the admittance matrices of the open (CPW without CNT) and short (CPW without a gap) dummies. The device under test (DUT), i.e., CNTs data can then be obtained by converting the admittance (Y) to S- or impedance (Z) data using standard conversion equations.[20] The transmission coefficient (S_{21}) S- parameter results obtained at room and 77 K temperatures are shown in Fig. 1(c). To ensure improved accuracy and reproducibility of the results, measurements were repeated several times and we used two probes. Instrument calibration was also done at the relevant temperatures. Making use of the transmission coefficient rather than the reflection coefficient (S_{11} or S_{22}) is known to improve the accuracy because S_{12} or S_{21} have higher signal-to-noise ratio (SNR) compared to S_{11} or S_{22}, especially in cases when there is load mismatch.[17]

The sample DW2 has eleven individual DWNTs aligned across the wave guide gap, while sample DW1 has four DWNTs see Fig. 1(a). The average outer diameter of each DWNT was about 2.0 nm see Fig. 1(b) and Ref. 15. After subtracting the Open dummy signal, it is observed that the aligned DWNTs alone transmit on average 3 dB at room temperature and about 6 dB at 77 K. The maximum measurement uncertainty at high frequencies ($\sim$ 50 GHz) was about 0.06 dB, this translates into a SNR of about 50 dB at room temperature and is even higher at low temperature.[17] Such a high SNR is significant to make sensible conclusions about individual HF responses of CNTs especially after repeatable measurement. From Fig. 1(c), it is observed that the eleven DWNTs of DW2 transmit on average about 2 dB more power than the four DWNTs of DW1 device at higher frequencies. A reduction in temperature is evidently accompanied by approximately 9 dB increase in transmission at high frequencies. Furthermore, the low temperature data show transmission saturation at around 40 GHz, which is not observed in the room temperature data. To understand the significance of temperature on the transmission capabilities of the devices, the complex impedance was extracted as outlined earlier.

Figures 2(a)–2(c) show a general decrease of real impedance (Z) with temperature particularly in the frequency range between 1 GHz and 25 GHz. This reduction in the resistive component of the impedance explains the increase in power transmission observed in Fig. 1(c). A comparative study of Figures 2(a)–2(c) shows a transition from capacitive (negative Z) to inductive (positive Z) behavior with a decrease in temperature. The implication of this capacitive to inductive transition can be understood through the realisation that the impedance of this quasi 1D transmission line (TL) network can be expressed as:

$$Z(\omega)^{-1} = \frac{i\omega C}{1 + i\omega RC - \omega^2 LC} + \frac{1}{R_0 + i\omega L_0}, \quad (3)$$

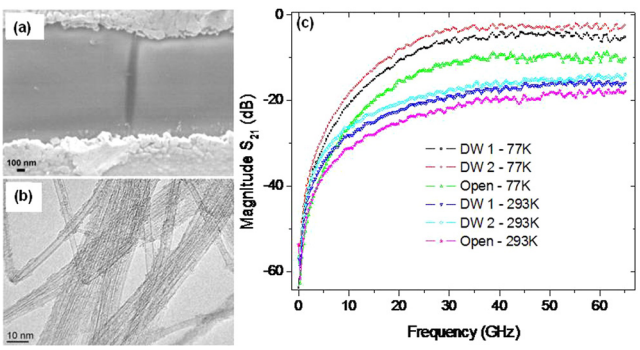

FIG. 1. (a) SEM micrograph of DW1; four DWNTs on separate positions, but because of the scale, only one can be seen. (b) TEM micrograph of DWNTs after catalyst removal and before alignment, showing good quality CNTs with small-diameter bundles. (c) Transmission coefficient for samples DW1 and DW2 at room and 77 K temperatures. The Open data are for the waveguides without CNTs aligned on them and is used to de-embed the parasitic effects.

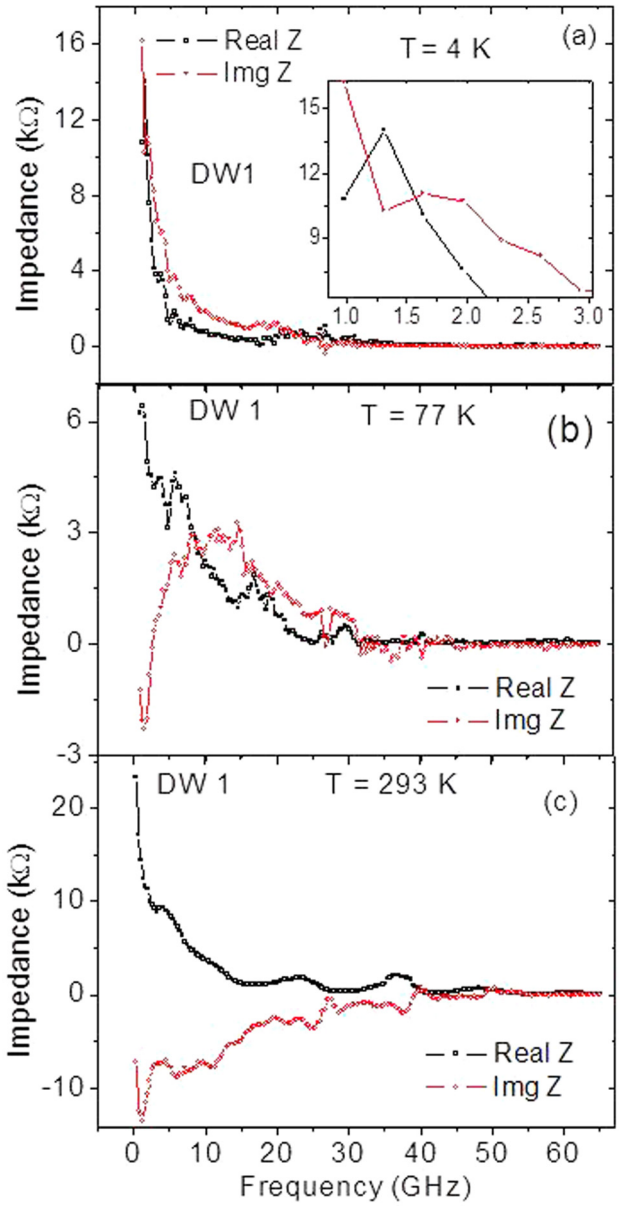

FIG. 2. Complex impedance of DW1 shows a transition from diffusive to ballistic transport (a) at about 1.5 GHz measured at 4 K. (b) at around 9 GHz measured at 77 K. (c) Room temperature measurements do not show any crossover to ballistic transport as was observed from other devices.

where R, C, and L are the resistance, capacitance, and inductance of the TL, respectively.[21] When the impedance becomes inductive, it means $LC \gg RC$, and Eq. (3) reduces to $Z(\omega) = R_0 + i\omega L_0$. R_0 can be regarded as the intrinsic CNT resistance plus the contact resistance. Now, using expressions for $\sigma(\omega)$ and $Z(\omega)$, when the real impedance is equal to the imaginary impedance, this corresponds to the point when $\omega\tau = 1$ if the contact resistance is neglected. This point will therefore signal the crossover point from diffusive $\omega\tau < 1$ to ballistic transport $\omega\tau > 1$. Therefore, plotting the two parts of the impedance on the same axis we see the significance of the capacitive to inductive response as shown in Figs. 2(a)–2(c). Similar results were also observed for other samples (not shown here).[22] Figures 2(a) and 2(b) show transitions from diffusive to ballistic transport at 1.5 GHz and 9 GHz, which correspond to 106 ps and 17 ps of momentum scattering time, respectively, provided that the contact resistance is neglected.

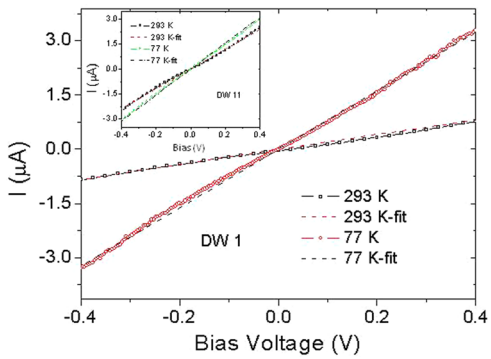

FIG. 3. I-V measurements for sample DW1 and DW11 (inset) fitted with the Landauer–Büttiker equation to determine the CNT – electrode coupling strength.

In the event of significant scattering in the CNTs, ballistic transport can still be realised when the scattering rate is less than the stimulus frequency.

In order to probe the origin of the capacitive to inductive transition as the temperature is reduced, we realise that previous theoretical[9,23] and experimental[24–26] works have predicted and observed a similar capacitive to inductive transition, which was explained in terms of the coupling strength between the electrodes and the CNT devices. To have an idea on this coupling, we fitted the two terminal I-V data with the Landauer–Büttiker formula in Eq. (1), see Fig. 3. The coupling strength of DW1 increased by 1.9 meV, by reducing the temperature to 77 K, similarly, for DW11 (one of the eleventh device with five CNTs), it increased by 1.2 meV. This increase is associated with a decrease in the contact resistance, and this probably explains the increase in high frequency transmission observed earlier in Fig. 1(a). To confirm this observation, we simulated the measured S-parameters using MATLAB RF Simulink package to determine the device parameters given in Fig. 4.

From the fitting of both the low temperature (Fig. 4, inset) and room temperature (Fig. 4) data, we observed a pronounced change in the contact resistance (R_3&R_2 of Fig. 5) by reducing temperature. The results show a small change of the CNT intrinsic high frequency parameters (R_4, L_1, and C_2 of the equivalent circuit in Fig. 5) with temperature. The

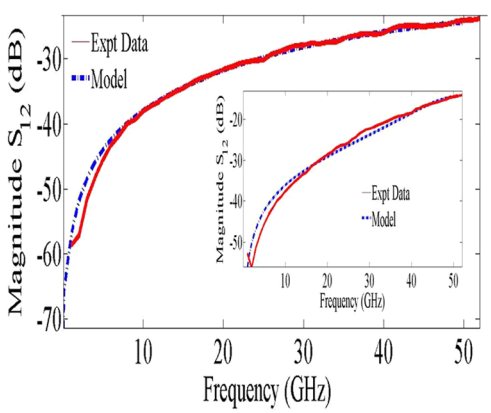

FIG. 4. The transmission coefficient S_{12} at 293 K for sample DW1, fitted with simulation model so as to determine the circuit parameters. Inset: The transmission coefficient S_{12} at 77 K for sample DW1, fitted with simulation model.

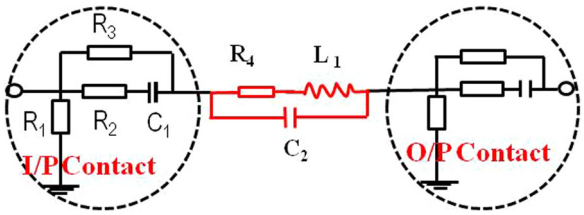

FIG. 5. Equivalent circuit model used for simulating the measured S – parameters. R_4, L_1, and C_2 are the intrinsic parameters of the CNTs.

TABLE I. The extracted circuit parameters from the fitting of DW1 S-parameters.

Parameter	Value at $T = 293$ K	Value at $T = 77$ K
R_1 (MΩ)	10	10
R_2 (Ω)	110	10
R_3 (kΩ)	90	90
R_4 (kΩ/μm)	1.2	0.4
C_1 (fF)	4.2	8
C_2 (fF/μm)	50	6
L_1 (nH/μm)	3.0	4.1

schematic circuit diagram in Fig. 5 was used to simulate the measured *S*-parameter results. Components R_3 and R_2 are associated with the contact and probe pad resistance. C_1 is the contact capacitance and R_1 is the signal–ground resistance. The contact circuit components were found to be symmetric for both input and output terminals as it was with the *S*-parameters results. Table I shows the extracted circuit component parameters from the fitting of Fig. 4. It can be seen that the simulation model fit slightly deviates from data at the low frequency regime particularly below 10 GHz of our devices. The exact reason for this is not yet clear but may be due to the fact that it is not easy to find a calibration technique with a very wide band frequency spectrum from 10 MHz to 65 GHz.

Our results in AC transport are consistent with previous DC measurements.[5,10,11] In the well-aligned tubes, current is parallel to the length of the tubes showing 1D transport instead of variable range hopping in three-dimensions. If the tubes are not perfectly aligned, the effect of the defect centres created at the overlapping points of the DWNTs may lead to 3D VRH transport. We have not seen any distinct effect of 3D VRH but only quasi-1D effect and therefore reveal that the tube-tube interactions is minimized here.

In conclusion, the reactive impedance of DWNTs show pronounced sensitivity to temperature changes resulting in a transition from capacitive to inductive response as the temperature is lowered. This crossover is due to a significant reduction in the contact resistance and thus enhancing the electrode-DWNT coupling. The implication of this is that the contact barrier and capacitance are reduced resulting in the crossover to inductive response and more power transmission at low temperature. In this work, we have established an impedance crossover at low temperatures due to contact effects, and thus, device engineers may consider incorporation of this in their designs. We believe that this work further motivates renewed search for transparent contacts on carbon based materials, so that modern technology can make use of ballistic transport achievable in CNTs.

S.B. acknowledges CSIR-NLC rental pool for establishing the laser deposition technique in our laboratory and NRF(SA) for NNEP and nanotechnology flagship grants.

[1]J. M. Bonard, T. Stora, J. P. Salvetat, F. Maier, T. Stoeckli, C. Duschl, L. Forro, W. A. de Heer, and A. Chatelaine, Adv. Mater. **9**, 827 (1997).
[2]P. X. Hou, S. Bai, Q. H. Yang, C. Lui, and H. M. Cheng, Carbon **40**, 81 (2002).
[3]P. Poncharal, C. Berger, Y. Yi, Z. L. Wang, and W. A. de Heer, J. Phys. Chem. B **106**, 12104 (2002).
[4]S. Fratini and F. Guinea, Phys. Rev. B **77**, 195415 (2008).
[5]C. L. Pint, Y. Q. Xu, E. Morosan, and R. H. Hauge, Appl. Phys. Lett. **94**, 182107 (2009).
[6]G. Chimowa, M. Sendova, E. Flahaut, D. Churochkin, and S. Bhattacharyya, J. Appl. Phys. **110**, 123708 (2011).
[7]S. Krishnan, H. Yilmaz, R. Vadapoo, and C. Marin, Appl. Phys. Lett. **97**, 163107 (2010).
[8]T. Shimada and T. Sugai, Appl. Phys. Lett. **84**, 2412 (2004).
[9]S. Pacchini, E. Flahaut, N. Fabre, V. Conedera, F. Mesnilgrente, F. Coccetti, M. Dragon, and R. Plana, Int. J. Microwave Wireless Tech. **2**, 471 (2010).
[10]X. He, N. Fujimura, J. M. Lloyd, K. J. Erickson, A. A. Talin, Q. Zhang, W. Gao, Q. Jiang, Y. Kawano, R. H. Hauge *et al.*, Nano Lett. **14**, 3953 (2014).
[11]C. Zhang, K. Bets, S. S. Lee, Z. Sun, F. Mirri, V. L. Colvin, B. I. Yakobson, J. M. Tour, and R. H. Hauge, ACS Nano **6**, 6023 (2012).
[12]P. J. Burke, IEEE Trans. Nanotechnol. **1**, 129 (2002).
[13]S. Kang, P. J. Burke, L. N. Pfeiffer, and K. W. West, Solid State Electron. **48**, 2013 (2004).
[14]S. Datta, *Electrical Transport in Mesoscopic Systems* (Cambridge University Press, Cambridge, UK, 1995).
[15]E. Flahaut, R. Bacsa, A. Peigney, and Ch. Laurent, Chem. Commun. (Cambridge) **12**, 1442 (2003).
[16]F. Seichepine, S. Salomon, M. Collet, S. Guillon, L. Nicu, G. Larrieu, E. Flahhaut, and C. Vieu, Nanotechnology **23**, 095303 (2012).
[17]See supplementary material at http://dx.doi.org/10.1063/1.4901025 for finer experimental details and error analysis.
[18]G. Chimowa and S. Bhattacharyya, AIP Adv. **4**, 087136 (2014).
[19]Q. Liang, J. D. Cressler, G. Niu, Y. Lu, G. Freeman, D. C. Ahlgen, R. M. Malladi, K. Newton, and D. L. Harame, IEEE Trans. Microwave Theory Tech. **51**, 2165 (2003).
[20]D. M. Pozar, *Microwave Engineering*, 4th ed. (John Wiley & Sons Inc, 1998).
[21]G. Cuniberti, M. Sassetti, and B. Kramer, Phys. Rev. B **57**, 1515 (1998).
[22]G. Chimowa, "Dynamic electrical Transport in carbon nanotubes and nanodiamond films," Ph.D. thesis (University of the Witwatersrand, Johannesburg, South Africa, 2014).
[23]T. Yamamoto, K. Sasaoka, and S. Watanabe, Phys. Rev. B **82**, 205404 (2010).
[24]M. Tsutsui, K. Kuno, S. Kurokwa, and A. Sakai, e-J. Surf. Sci. Nanotech. **5**, 12 (2007).
[25]V. K. Ksenevich, N. I. Gorbachuk, N. A. Poklonski, V. A. Samuilov, M. E. Kozlov, and A. D. Wieck, Fullerenes, Nanotubes, Carbon Nanostruct. **20**, 434 (2012).
[26]L. Gomez-Rojas, S. Bhattacharyya, E. Mendoza, D. C. Cox, J. M. Rosolen, and S. R. P. Silva, Nano Lett. **7**, 2672 (2007).